CL-170928 Received: September 30, 2017 | Accepted: November 4, 2017 | Web Released: November 15, 2017

Oxidation-promoted Interfacial Synthesis of Redox-active Bis(diimino)nickel Nanosheet

Eunice J H Phua,[1] Kuo-Hui Wu,[1] Keisuke Wada,[1] Tetsuro Kusamoto,[1] Hiroaki Maeda,[1] Jian Cao,[1] Ryota Sakamoto,[1] Hiroyasu Masunaga,[2] Sono Sasaki,[3,4] Jia-Wei Mei,[5,6] Wei Jiang,[6] Feng Liu,*[6] and Hiroshi Nishihara*[1]

[1]*Department of Chemistry, Graduate School of Science, The University of Tokyo, 7-3-1 Hongo, Bunkyo-ku, Tokyo 113-0033, Japan*
[2]*Japan Synchrotron Radiation Research Institute (JASRI)/SPring-8, 1-1-1 Kouto, Sayo-cho, Sayo-gun, Hyogo 679-5198, Japan*
[3]*Department of Fibre Science and Engineering, Kyoto Institute of Technology, 1 Matsugasaki Hashikami-cho, Sakyo-ku, Kyoto 606-8585, Japan*
[4]*RIKEN SPring-8 Centre, 1-1-1 Kouto, Sayo-cho, Sayo-gun, Hyogo 679-5148, Japan*
[5]*Beijing Computational Science Research Center, Beijing 100193, P. R. China*
[6]*Department of Materials Science and Engineering, University of Utah, Salt Lake, UT 84112, USA*

E-mail: nisihara@chem.s.u-tokyo.ac.jp (H. Nishihara), fliu@eng.utah.edu (F. Liu)

Bis(diimino)nickel (NiDI) nanosheet is prepared by two methods of oxidation-promoted interfacial coordination reactions of nickel(II) ions with hexaaminobenzene. The thickness of the large chemically formed NiDI nanosheet can be controlled from atomic layers to thousands of layers. The morphology of electrochemically formed NiDI-modified electrode achievable within a minute suggests longitudinal growth of nanosheets at the surface. Increasing capacity of the NiDI with its amount indicates NiDI as a promising energy storage material.

Keywords: Coordination nanosheet (CONASH) | Bis(diimino)nickel | Electropolymerization

Coordination nanosheets, or CONASHs, are two-dimensional molecular materials consisting of metal ions connected by bridging ligands via coordination bonds, which can be rationally designed and facilely synthesized in ambient conditions by a bottom-up method.[1] This approach holds great promise for developing novel materials with unexpected and tailorable properties based on the intrinsic nature of the electron delocalization over the infinite plane when strongly correlated electron systems are constructed using an appropriate combination of transition metals with π-conjugated bridging ligands.[1,2] The bottom-up approach of synthesizing two-dimensional (2D) coordination nanosheets (CONASHs) from their corresponding metal ions and organic ligands has proved its potential to form versatile and highly functional materials based on the redox-active, electrochromic, electroconductive, photoconductive, luminescent, catalytic, photo-electro conversion, and electrocapacitive properties as some of its examples.[3] Our previous research on bis(dithiolato)nickel (NiDT) nanosheet afforded film-like products with a kagome lattice and controllable thickness down to single-layer using facile gas/liquid and liquid/liquid interfacial coordination reactions. Their strongly correlated electronic properties include high electronic conductivity of 160 S cm^{-1} and the prediction of single-layer NiDT to be a 2D topological insulator.[4] We have recently reported bis(iminothiolato)nickel (NiIT)[5] nanosheet, which is isoelectronic to NiDT and has conductivity of 0.1 S cm^{-1}. Our investigation of bis(diimino)nickel (NiDI) nanosheets (Figure 1a), also an isoelectronic structure of NiDT and known to have oxidation states of −1, 0, +1,[6] began much earlier. The NiDI nanosheets were recently described by Lahiri et al.[7] and Dou et al.[8] Part of our research is more similar to the recent paper by Dou et al. but here we would like to share some additional data

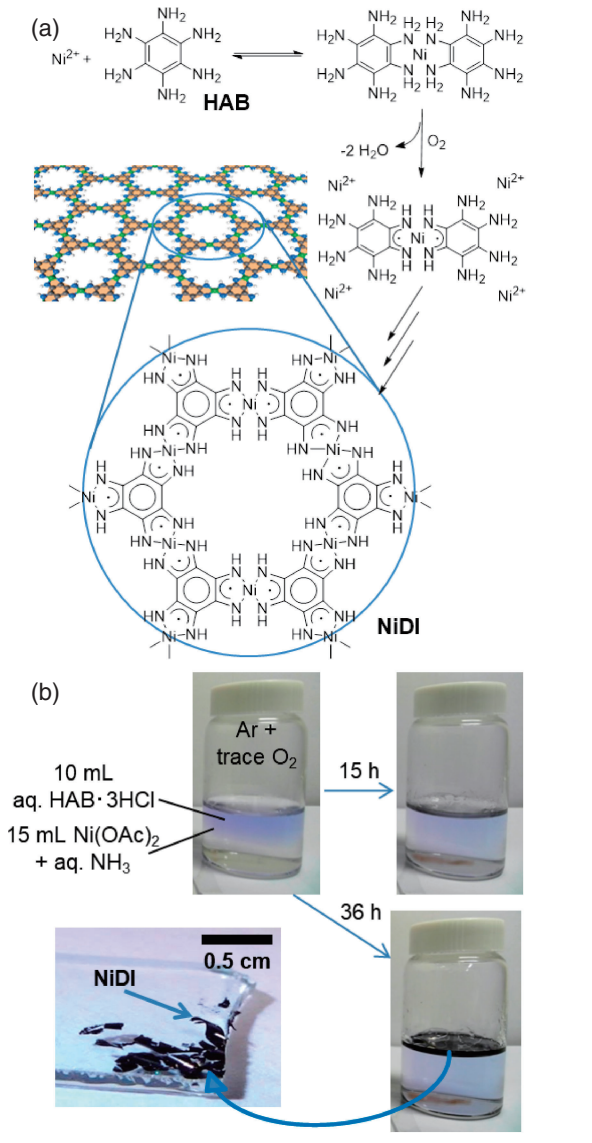

Figure 1. Formation of chemically synthesized NiDI. (a) Mechanism of NiDI formation and the resulting kagome lattice. (b) Reaction conditions and gradual formation of NiDI sheet with oxidation, resulting crystalline NiDI transferred onto glass substrate.

as well as a novel electrochemical method to fabricate a redox-active and highly electrocapacitive NiDI-modified electrode.

The liquid/liquid interfacial coordination reaction that we employed for the synthesis of NiDT nanosheet in 2013[4] has been applied for the preparation of several other CONASHs in our group as well as by other researchers. Similar to Dou et al., we found the reaction of this system to be inefficient unless oxygen gas is introduced. Oxygen is required for the biradical formation in hexaaminobenzene (HAB) with structures similar to Ni_3(2,3,6,7,10,11-hexaiminotriphenylene)$_2$ or bis(*o*-diiminobenzosemiquinonato)nickel(II), Ni(isq)$_2$ (isq: *o*-diiminobenzosemiquinonato), which are synthesized under air.[6,8,9] Hence, our optimized synthesis of the NIDI nanosheet uses an oxidation-assisted reaction with aqueous HAB·3HCl ligand (0.4 mM) and nickel(II) acetate (Ni(OAc)$_2$) (15 mM) in 4.5 M excess concentrated ammonia solution at room temperature (see Supporting Information, section 1.2 and Figure 1b). The sheet slowly forms on the calm liquid surface in contact with air-containing argon over time (Figure S1). We propose a plausible mechanism in Figure 1a. In the as-prepared solution, two HAB ligands neutralized by ammonia reversibly coordinate to the nickel ion due to the weak coordination ability of anilines. As dioxygen is introduced, a pair of coordinated amines on the ligand undergo oxidation, which dramatically improves the coordination ability, resulting in a stabilized π-conjugated five-membered metallacycle. Henceforth, the other free amines on the ligand similarly coordinate to other nickel ions, which sequentially coordinate with other ligands. Eventually, the complexes expand to become a large crystalline NiDI nanosheet with a metallic luster on the gas/liquid interface as seen in Figure 1b. This sheet forms a kagome lattice similar to the illustration in Figure 1a. Thicknesses of the crystalline black sheets depend on the rates and amount of dioxygen introduced into the gas phase just above the reaction solution.

The NiDI sheet obtained was characterized using XPS (Figure S2), IR spectroscopy (Figure S3), and powder X-ray diffraction (pXRD) and found to be similar to the highly crystalline version of Dou et al. with $a = b = 13.01$ Å and $c = 3.25$ Å (Figure S4). The NiDI samples made using this method were capable of slower reaction rate as it is synthesized at room temperature. Large (centimeter-scale) and thick crystalline NiDI sheets spanning the entire aqueous surface of the reaction vessel can be obtained if the setup is undisturbed. 1 cm^2 of thick NiDI sheets can be easily synthesized and these were characterized using SEM (Figure 2a) and TEM (Figure 2b). By controlling the rates and amount of dioxygen, we obtained differing thicknesses of NiDI as observed by AFM. Partly due to the limitations of AFM, the thickest film we measured was 2.7 µm, corresponding to more than three thousand layers. With the reduction of exposure time to dioxygen, the thickness of the NiDI sheets detected was reduced from approximately 20 nm-thick (Figure 2c) to just 0.8 nm-thick at its edges (Figure 2d), corresponding to the first detection of a single layer NiDI nanosheet.

Our DFT calculations (Figure S5) showed metallic behavior similar to the results of Dou et al. The electrical conductivity of the chemically prepared NiDI nanosheet in its pelletized form was measured using a four-terminal method under helium was found to be in between that found by Lahiri et al. and Dou et al. (Figure S6). Since this has already been explained by Dou et al.

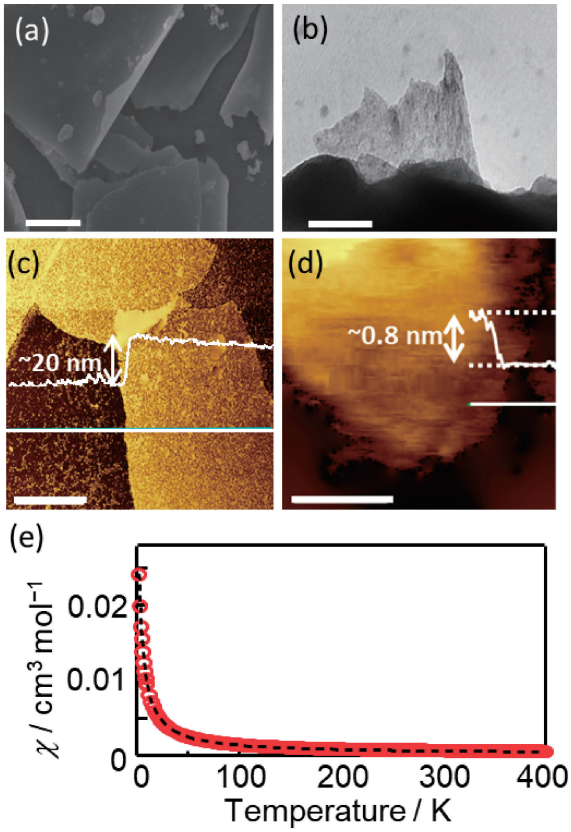

Figure 2. Characterization and NiDI properties. (a) SEM image of NiDI. Scale bar represents 5 µm. (b) TEM image of NiDI. Scale bar represents 100 nm. (c) AFM height topography image of 20 nm NiDI. Scale bar represents 5 µm. (d) AFM height topography image of the edge of NiDI showing a single layer of 0.8 nm monolayer. Scale bar represents 50 nm. (e) Temperature-dependent magnetic susceptibility of NiDI. The dotted line is the fitting curve of $\chi(T) = C(T-\theta)^{-1} + \chi_0$ using the parameter $\chi_0 = 1.9 \times 10^{-4}$ cm^3 mol^{-1}, $C = 0.12$ cm^3 K mol^{-1} and $\theta = -3.0$ K.

to be due to the crystallinity of the samples, this paper will not be focusing on these.

Magnetic investigations of the chemically prepared NiDI nanosheet using superconducting quantum interference device (SQUID) revealed the existence of non-negligible magnetic moments (Figure 2e), while neutral Ni(isq)$_2$, a fundamental constituted unit of the NiDI nanosheet, forms a non-magnetic singlet state.[6,10] The simulation of the magnetic susceptibility $\chi(T)$ from 2 to 400 K using the formula $\chi(T) = C(T-\theta)^{-1} + \chi_0$ (Curie–Weiss term $C(T-\theta)^{-1}$ with temperature-independent term χ_0) afforded Curie constant $C = 0.12$ cm^3 K mol^{-1} and Weiss temperature $\theta = -3.0$ K, suggesting the existence of local magnetic moments with antiferromagnetic interactions. The existence of these magnetic moments is very interesting but more investigation is required before any substantial conclusions can be made.

Discovering the necessity of oxidation, we developed another synthetic method using electrochemical oxidation, which produces the NiDI nanosheet directly on an electrode surface. The electrochemical polymerization was carried out at an

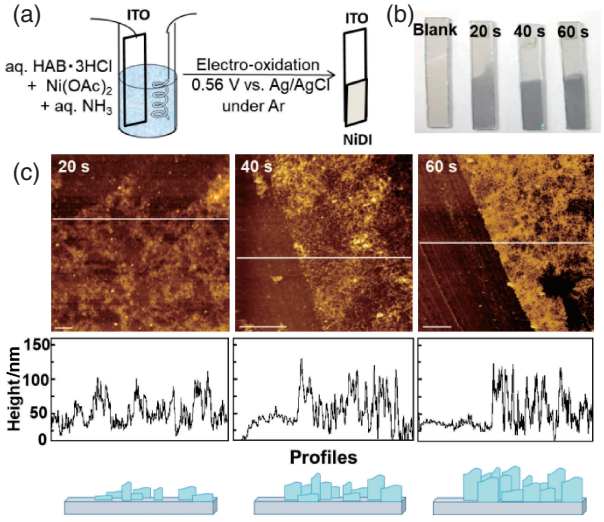

Figure 3. Synthesis and characterization of electrochemically synthesized NiDI. (a) Illustration of electrochemical setup of constant potential synthesis of NiDI on ITO. (b) Photo of blank ITO as compared to NiDI samples which has undergone 20, 40, and 60 s of constant potential of 0.56 V vs. Ag/AgCl. (c) Illustrations, AFM topography images and height profiles of scratched AFM samples obtained by 0.56 V for 20, 40, and 60 s, respectively. Scale bars represent 5 µm.

indium-tin oxide (ITO) glass in a HAB·3HCl–Ni(OAc)$_2$–NH$_3$ aqueous solution with 0.1 M $NaBF_4$ as electrolyte under an argon atmosphere (Figure 3a). A black film immediately formed and adhered strongly to the ITO electrode when 0.56 V vs. Ag/AgCl was applied to oxidize HAB. In comparison, electro-oxidation of nickel-free reaction solution (HAB·3HCl–NH_3–$NaBF_4$) afforded no film on the electrode, indicating the role of nickel ions for the polymerization. The electrochemically prepared black film identified by XPS (Figure S7), IR (Figure S8), and pXRD (Figure S9), confirms an identical chemical structure with the chemically synthesized NiDI nanosheet but with lower crystallinity. This less ordered structure of electrochemically prepared NiDI results from the quick formation and the difference of the reaction field (solid–liquid interface for the electropolymerization versus gas–liquid interface for the chemical polymerization). We propose that this electropolymerization proceeds through a mechanism identical to the dioxygen-assisted sheet formation.

This electrochemical method enables a more controllable growth of the nanosheet as compared to the gas–liquid interfacial reaction as the degree of oxidation can be precisely adjusted. A series of samples with synthetic times varying from 10 to 60 s were synthesized (Figure 3b), and their UV–vis–NIR absorption spectra and AFM images were obtained. Representative scratched samples with synthetic times of 20, 40, and 60 s, show nonplanar and jagged surfaces from their AFM topographical images. The empty spaces (blank ITO without NiDI) decreased while the topographical height increased gradually with time. This indicates the growth of perpendicularly deposited NiDI nanosheets which is as illustrated by the illustration below each of the height profiles (Figure 3c). After 60 s, the average thickness of the NiDI film was 75 nm.

UV–vis–NIR absorption spectra exhibit a broad peak over 700–1500 nm with λ_{max} = ca. 1060 nm (Figure 4a). The absorbance of the respective samples at 1060 nm increases nonlinearly with time, corresponding approximately to the charge vs. time graph for each of the respective samples during cyclic voltammetry (see section on cyclic voltammetry), as well as the gradual increase of the charge consumed during their syntheses, using a 60 s sample as an example (Figure 4b). This nonlinear increase corresponds to the previous hypothesis of the perpendicular growth of NiDI on the ITO electrodes as described in the previous section.

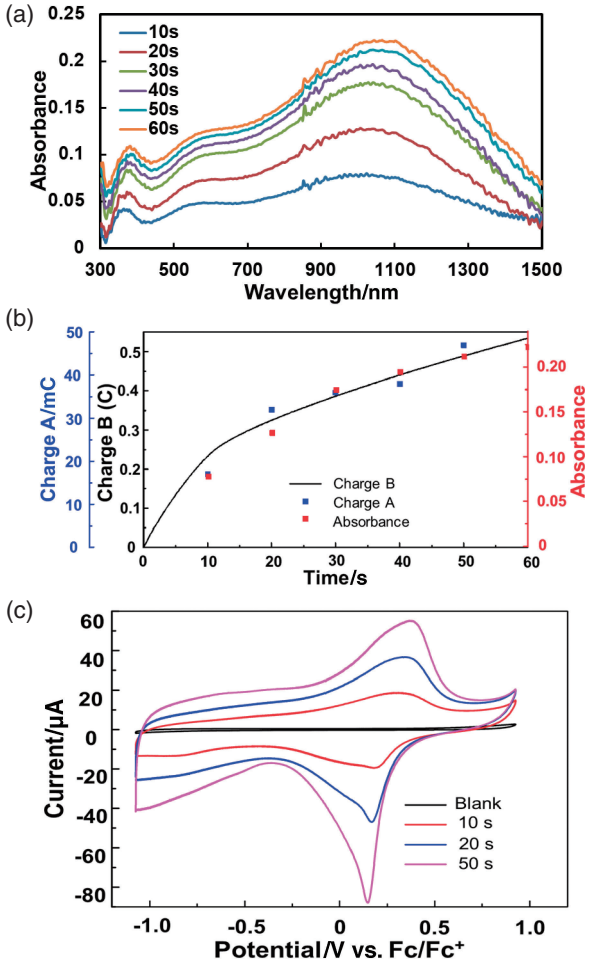

Figure 4. Properties of electrochemically synthesized NiDI. (a) UV–vis–NIR absorption spectra of electrochemically synthesized NIDI by constant potential electrolysis at 0.56 V vs. Ag/AgCl in a HAB·3HCl–Ni(OAc)$_2$–NH_3 aqueous solution with 0.1 M $NaBF_4$ under Ar for 10 to 60 s respectively. (b) Absorbance at λ_{max} of the samples synthesized by differing durations corresponding to the charge A, the electro activity charges, and charge B, the charge obtained during the synthesis of the sample with 60 s of 0.56 V vs. Ag/AgCl constant potential. (c) Cyclic voltammograms showing increasing capacity of NiDI with increasing synthetic timings of 10, 20, and 50 s respectively as compared to blank ITO.

Redox activities of both chemically and electrochemically synthesized NiDI nanosheets were investigated using cyclic voltammetry (CV) in 1 M Bu_4NClO_4–MeCN. Both NiDI nanosheets exhibit peak couples at approximately 0.28 V vs. ferrocene/ferrocenium (Fc/Fc^+) with chemical reversibility

(Figure 4c and Figure S10). This peak couple can be ascribed to $[NiDI]^{+}/[NiDI]^{0}$ based on the redox behavior of the mononuclear bis(diimino)nickel complex. Cyclic voltammograms of electrochemically prepared NiDI nanosheet on ITO exhibit not only faradaic currents but also very large charging currents. The amount of charge gained from each sample with increasing synthetic duration during its CV has been plotted against time in Figure 4b. Representative cyclic voltammograms plotted together show an increase in the charge capacity with the increase in synthetic time, which also means an increase in charge capacity with the amount of NiDI (Figure 4c). This, together with its stable redox behavior and electrical conductivity, reveals its potential for applications for charge storage. It should also be mentioned that the chemically oxidized film also gives the same redox behavior.

In conclusion, we have successfully used two separate methods of slow oxidation and controlled oxidation to synthesize and characterize NiDI. Magnetic studies of bulk NiDI show local magnetic moments with antiferromagnetic interaction. Chemically reversible redox active NiDI indicates its potential as an energy storage material. We believe that the possibility of fine-tuning chemical structures and properties remains to be one of the greatest advantages for the utilization of NiDI and its family of CONASHs as electronic and electrochemically functional materials.

This work is supported by JST-CREST JPMJCR15F2, and JSPS KAKENHI Grant Numbers JP15H00862, JP15J06673, JP15K13654, JP16H00900, JP16H00957, JP26220801, JP26708005, JP17H05354, JP17H03028. Work at Utah is supported by US Department of Energy (Grant No. DE FG02-04ER46148). The synchrotron radiation experiments were performed at BL45XU in SPring-8 with the approval of RIKEN (Proposal No. 20160041). Part of this work was performed using facilities of the Cryogenic Research Center, the University of Tokyo. XPS measurements were conducted at Advanced Characterization Nanotechnology Platform of the University of Tokyo, supported by "Nanotechnology Platform" of the Ministry of Education, Culture, Sports, Science and Technology (MEXT), Japan. We acknowledge NERSC and CHPC at the University of Utah for providing the computing resources. EP acknowledges Research Fellowships of Japan Society for the Promotion of Science (JSPS) for Young Scientists and the Materials Education Program for the Future Leaders in Research, Industry, and Technology (MERIT).

Supporting Information is available on http://dx.doi.org/10.1246/cl.170928.

References

1 a) R. Sakamoto, K. Takada, X. Sun, T. Pal, T. Tsukamoto, E. J. H. Phua, A. Rapakousiou, K. Hoshiko, H. Nishihara, *Coord. Chem. Rev.* **2016**, *320–321*, 118. b) H. Maeda, R. Sakamoto, H. Nishihara, *Langmuir* **2016**, *32*, 2527.
2 N. S. Hush, *Coord. Chem. Rev.* **1985**, *64*, 135.
3 a) X.-H. Liu, C.-Z. Guan, D. Wang, L.-J. Wan, *Adv. Mater.* **2014**, *26*, 6912. b) Y. Xu, A. Nagai, D. Jiang, *Chem. Commun.* **2013**, *49*, 1591. c) R. Sakamoto, K. Hoshiko, Q. Liu, T. Yagi, T. Nagayama, S. Kusaka, M. Tsuchiya, Y. Kitagawa, W.-Y. Wong, H. Nishihara, *Nat. Commun.* **2015**, *6*, 6713. d) K. Takada, R. Sakamoto, S.-T. Yi, S. Katagiri, T. Kambe, H. Nishihara, *J. Am. Chem. Soc.* **2015**, *137*, 4681. e) M. C. Aragoni, M. Arca, T. Cassano, C. Denotti, F. A. Devillanova, F. Isaia, V. Lippolis, D. Natali, L. Nitti, M. Sampietro, R. Tommasi, G. Verani, *Inorg. Chem. Commun.* **2002**, *5*, 869. f) T. Pal, T. Kambe, T. Kusamoto, M. L. Foo, R. Matsuoka, R. Sakamoto, H. Nishihara, *ChemPlusChem* **2015**, *80*, 1255.
4 a) T. Kambe, R. Sakamoto, K. Hoshiko, K. Takada, M. Miyachi, J.-H. Ryu, S. Sasaki, J. Kim, K. Nakazato, M. Takata, H. Nishihara, *J. Am. Chem. Soc.* **2013**, *135*, 2462. b) T. Kambe, R. Sakamoto, T. Kusamoto, T. Pal, N. Fukui, K. Hoshiko, T. Shimojima, Z. Wang, T. Hirahara, K. Ishizaka, S. Hasegawa, F. Liu, H. Nishihara, *J. Am. Chem. Soc.* **2014**, *136*, 14357.
5 X. Sun, K.-H. Wu, R. Sakamoto, T. Kusamoto, H. Maeda, H. Nishihara, *Chem. Lett.* **2017**, *46*, 1072.
6 a) A. L. Balch, R. H. Holm, *J. Am. Chem. Soc.* **1966**, *88*, 5201. b) D. Herebian, E. Bothe, F. Neese, T. Weyhermüller, K. Wieghardt, *J. Am. Chem. Soc.* **2003**, *125*, 9116.
7 N. Lahiri, N. Lotfizadeh, R. Tsuchikawa, V. V. Deshpande, J. Louie, *J. Am. Chem. Soc.* **2017**, *139*, 19.
8 J.-H. Dou, L. Sun, Y. Ge, W. Li, C. H. Hendon, J. Li, S. Gul, J. Yano, E. A. Stach, M. Dincă, *J. Am. Chem. Soc.* **2017**, *139*, 13608.
9 D. Sheberla, L. Sun, M. A. Blood-Forsythe, S. Er, C. R. Wade, C. K. Brozek, A. Aspuru-Guzik, M. Dincă, *J. Am. Chem. Soc.* **2014**, *136*, 8859.
10 D. Herebian, K. E. Wieghardt, F. Neese, *J. Am. Chem. Soc.* **2003**, *125*, 10997.

